Geophysical Prospecting **36**, 223–243, 1988

A METHOD FOR DETERMINATION OF VELOCITY AND DEPTH FROM SEISMIC REFLECTION DATA[1]

E. LANDA[2], D. KOSLOFF[3], S. KEYDAR[2], Z. KOREN[3] and M. RESHEF[4]

ABSTRACT

LANDA, E., KOSLOFF, D., KEYDAR, S., KOREN, Z. and RESHEF, M. 1988. A method for determination of velocity and depth from seismic reflection data. *Geophysical Prospecting* **36**, 223–243.

The estimation of velocity and depth is an important stage in seismic data processing and interpretation. We present a method for velocity–depth model estimation from unstacked data. This method is formulated as an iterative algorithm producing a model which maximizes some measure of coherency computed along traveltimes generated by tracing rays through the model. In the model the interfaces are represented as cubic splines and it is assumed that the velocity in each layer is constant. The inversion includes the determination of the velocities in all the layers and the location of the spline knots.

The process input consists of unstacked seismic data and an initial velocity–depth model. This model is often based on nearby well information and an interpretation of the stacked section.

Inversion is performed iteratively layer after layer; during each iteration synthetic traveltime curves are calculated for the interface under consideration. A functional characterizing the main correlation properties of the wavefield is then formed along the synthetic arrival times. It is assumed that the functional reaches a maximum value when the synthetic arrival time curves match the arrival times of the events on the field gathers. The maximum value of the functional is obtained by an effective algorithm of non-linear programming.

The present inversion algorithm has the advantages that event picking on the unstacked data is not required and is not based on curve fitting of hyperbolic approximations of the arrival times. The method has been successfully applied to both synthetic and field data.

1. INTRODUCTION

The estimation of velocity and depth is an important stage in seismic data processing and interpretation. Depth is usually estimated by converting zero-offset

[1] Paper read at the 48th EAEG meeting, Ostend, June 1986; accepted for publication September 1987.

[2] The Institute for Petroleum Research and Geophysics, P.O. Box 2286, Holon 58120, Israel.

[3] Department of Geophysics, Tel Aviv University, Ramat Aviv, Israel.

[4] Cray Research Inc., 1440 Northland Drive, Mendota Heights, MN 55120, U.S.A.

traveltimes interpreted from a stacked section to depth, using a velocity field obtained from a normal moveout (NMO) analysis. This method requires an accurate representation of the root-mean-square (RMS) velocity field. However, the stacking velocities used for such analyses can deviate significantly from RMS velocities, since analyses of stacking velocities assume that the medium is laterally invariant and that traveltime trajectories for reflection events in common depth point (CDP) gathers are hyperbolic.

Estimation of reflector depth and interval velocity from seismic reflection data may be formulated as an inverse problem. Considerable work has been done recently in full wavefield linearized inversion of multi-offset seismic data (Clayton and Stolt 1981; Berkhout 1984; Tarantola 1984a; Bleistein, Cohen and Magin 1985; Ikelle, Diet and Tarantola 1986). Non-linear inversion techniques (Tarantola 1984b, 1986; McAulay 1985; Gauthier, Virieux and Tarantola 1986) show much promise, but they are still in the formulative stages. A more complete review of inversion of seismic data can be found by Stolt and Weglein (1985).

Another approach to inversion of seismic data has been proposed by Goldin (1979), Gjoystdal and Ursin (1981) and Bishop *et al.* (1985). This method is called 'seismic tomography' and is formulated as an iterative algorithm producing a velocity–depth model which minimizes the difference between traveltimes generated by tracing rays through the model and traveltimes measured from the data. The input to this process consists of traveltimes measured from selected events on unstacked seismic data. The disadvantage of these methods is that with a small signal-to-noise ratio, event picking on unstacked data is not a reliable process and leads to the failure of the inverse procedure.

We propose a new method for velocity–depth model estimation from unstacked seismic data, which has the advantage that it does not require event picking on unstacked data and it is not based on curve fitting or hyperbolic approximations of arrival times. The method is formulated as an optimization algorithm producing a velocity–depth model, which maximizes some measure of coherency computed for unstacked trace gathers in a time window along traveltime curves generated by ray tracing through the model. The inversion includes the determination of velocities in all the layers and the location of interfaces.

The input includes unstacked seismic data (common midpoint (CMP) gathers or common shot gathers) and an initial velocity–depth model. This model is often based on nearby well information and an interpretation of the stacked section. Inversion is performed iteratively layer after layer and, during each iteration, synthetic traveltime curves are calculated for the interface under consideration. A functional characterizing the main correlation properties of the wavefield is then formed along the synthetic arrival times. It is assumed that this functional reaches a maximum value when the synthetic arrival time curves match the arrival times of the events on the field gathers. The maximum value of the functional is obtained by an algorithm of non-linear programming. Figure 1 shows the block scheme of the algorithm. A similar approach of maximization of some measure of coherency for velocity analysis without picking and statics estimation was suggested by Toldi (1985), Ronen and Claerbout (1985) and Rothman (1985). Their methods are based

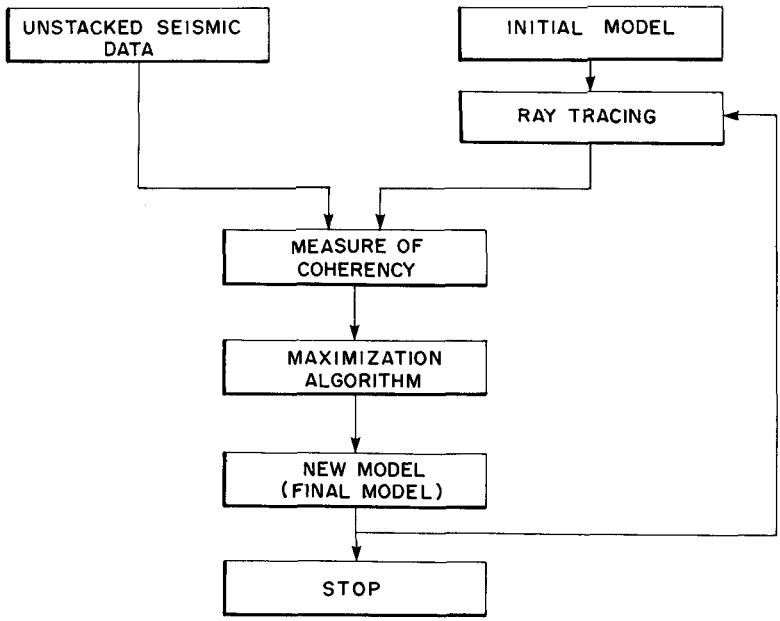

FIG. 1. Scheme of the algorithm.

essentially on the hyperbolic approximation of real CMP traveltime curves and on stack power.

In practice the optimization algorithm depends on: (1) an interpretative model of the medium, (2) an algorithm of ray tracing, (3) the choice of an objective function, and (4) a method for finding the maximum of the objective function. We will discuss each of these factors separately.

2. AN INTERPRETATIVE MODEL OF THE MEDIUM

We assume that the real medium can be adequately modelled as a series of homogeneous layers separated by interfaces across which the velocity can vary discontinuously. Let X be the horizontal distance along the earth's surface, Z the depth and N the number of layers (Fig. 2). The velocity v in each layer is assumed to be constant and the interfaces are represented as cubic splines which are determined by M nodepoints $Z_n(X_1), Z_n(X_2), \ldots, Z_n(X_M)$, $n = 1, \ldots, N$. For simplicity in the following discussion, we assume that the number of nodepoints is the same for each layer, although this is not essential. The assumption that the interval velocity does not change laterally within the layer does not hold in areas with complex geological structures and then we divide the region of interest into segments with constant interval velocities. The interpretative model can now be characterized by the vector

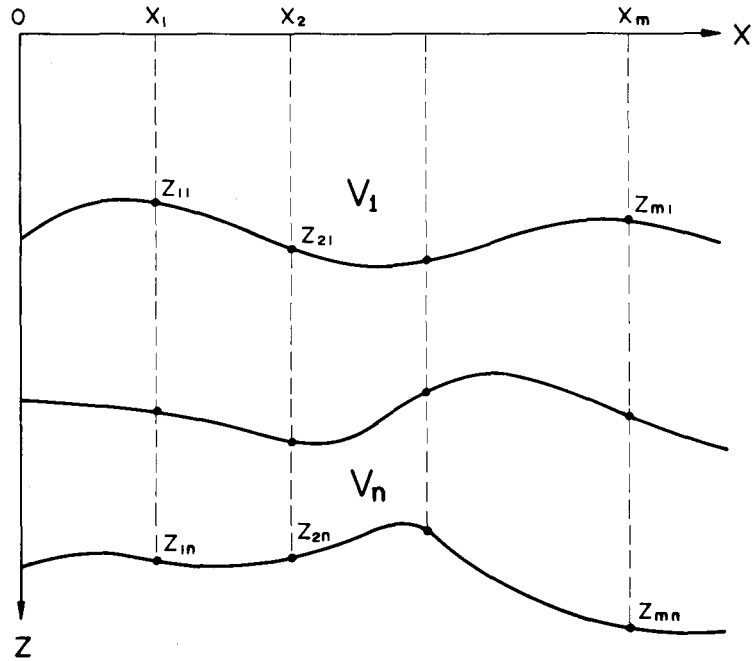

FIG. 2. Parameterization of the model.

of parameters $\boldsymbol{\theta}$:

$$\boldsymbol{\theta} = \{v_1, v_2, \ldots, v_N, Z_{11}Z_{21}, \ldots, Z_{1N}, Z_{2N}, \ldots, Z_{MN}\}, \tag{1}$$

where v_n is the interval velocity in the nth layer, and Z_{mn} the depth of the nth layer in the mth nodepoint with coordinate X.

The dimension of the vector $\boldsymbol{\theta}$ should be sufficiently high to accurately describe the real earth; however, it should not be so high that the inversion problem becomes intractable or indeterminate.

In addition to $\boldsymbol{\theta}$, which describes the model, we need to describe the inversion data set. The data consist of a wavefield registered in a time window around the synthetic traveltime curves computed for the model. Let there be I shots with a maximum of J geophones per shot and suppose that the arrival time of the nth reflected wave to the receiver j from the source i is $\tau_{ijn}(\boldsymbol{\theta})$. The observed wavefield in discrete form is represented as U_{ij} $(t_{ijnk}, \boldsymbol{\theta})$, where $k = 1, \ldots, K$; $K\,\Delta t$ is a time window; Δt is a sample interval and $\tau_{ijn} < t_{ijnk} < \tau_{ijn} + K\,\Delta t$. The total vector of the wavefield is called $\mathbf{U}(\boldsymbol{\theta})$.

3. RAY TRACING ALGORITHM

The optimization approach requires a large number of calculations of the objective function which is based here on the computation of arrival time curves. Therefore, a fast and reliable ray tracing algorithm is crucial for the proposed inversion method.

As a rule, the ray tracing algorithm comprises two main stages. One is the initial values problem, the parameterization of the subsurface model and the scheme of 'shooting the rays'; and the second is the boundary values problem which is finding the raypath and the traveltime at a certain point of observation. The classical method of solving these problems is the so-called 'two-point ray tracing method' which is based on the convergence of rays to certain receivers by an iterative procedure. An alternative approach is the 'interpolation method' which consists of shooting a small number of rays covering the area of interest and interpolating the traveltimes to the receiver positions.

We used a combination of these two approaches. In general, we prefer the interpolation method because of its speed. The forward modelling accuracy is achieved by using the 'two-point ray tracing method' in those regions where the arrival time curves become complicated.

Figure 3 shows an example of the interpolation approach for a two-layered model (b); the unbroken lines in Fig. 3a represent corresponding traveltime curves.

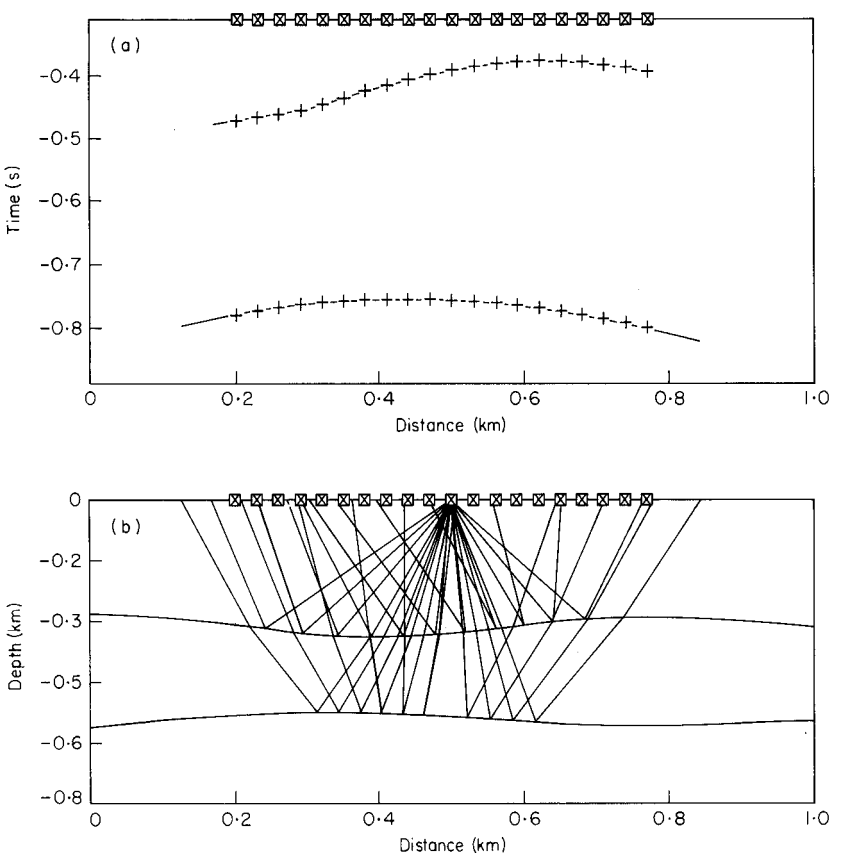

FIG. 3. 'Interpolation' ray tracing. (a) Traveltime curves, (+ + +) represent the exact solution. (b) Depth model and ray scheme.

Only ten rays were used for each layer. The + in Fig. 3a represents the exact solution obtained by two-point ray tracing. We had to shoot about 100 rays for each layer to obtain efficient convergence to receiver location.

4. Objective Function

Let there be some measure of coherency S which characterizes the main correlation properties of the wavefield. We propose the following criterion for a model estimation. For all shots (or midpoints) and reflectors, we can calculate the total measure of coherency along the traveltime trajectories generated by ray tracing. The larger this total sum of coherency, the better the model $\boldsymbol{\theta}$.

Therefore, the purpose of inversion is to find a model for which this measure S will be at a maximum, i.e. the problem is to find the function

$$\phi(\boldsymbol{\theta}) = \max_{\boldsymbol{\theta}} S(\boldsymbol{\theta}). \tag{2}$$

For computational reasons, it is more convenient to look for a minimum of the functional; therefore, we shall consider functions $\psi(\boldsymbol{\theta}) = -\phi(\boldsymbol{\theta})$ and will call them 'objective functions'.

Different measures of coherency can be taken as functional S. We adopted the semblance function (Neidell and Taner 1971) to estimate the presence or absence of a correlated signal along a calculated traveltime curve. The coherency properties of the nth reflected wave can be written as follows (Kong, Phinney and Roy-Chowdhury 1985):

$$S_n(\boldsymbol{\theta}) = \sum_{i=1}^{I} \frac{1}{K\,\Delta t} \sum_{k=1}^{+K} \frac{\{\sum_{j=1}^{J} U_{ij}(\tau_{ijn}(\boldsymbol{\theta}) + k\,\Delta t)\}^2}{J \sum_{j=1}^{J} U_{ij}^2(\tau_{ijn}(\boldsymbol{\theta}) + k\,\Delta t)}. \tag{3}$$

One of the main problems in non-linear inversion is the existence of more than one minimum in an objective function. To illustrate the behaviour of functional (3) graphically, we calculated (3) for a simple model with one horizontal layer. In this case the vector $\boldsymbol{\theta}$ has only two parameters, $\boldsymbol{\theta} = \{v, h\}$, where h is the thickness of the layer.

Figure 4a shows contours of the objective function $\psi = -S(\boldsymbol{\theta})$ for different combinations of parameters h and v; the true values were $v = 2000$ m/s and $h = 250$ m. In Fig. 4 the objective function has a simple character with a clear minimum which corresponds to the correct values of v and h.

Let us look at the structure of the objective function in the vicinity of the minimum (on a small scale, Fig. 4b). The complexity of the function and existence of local minima can lead to a decrease in the estimation precision of the parameter vector $\boldsymbol{\theta}$. Local minima occur when we calculate the semblance functional (3) in the vicinity of the global minimum along traveltime curves which are parallel to 'true'

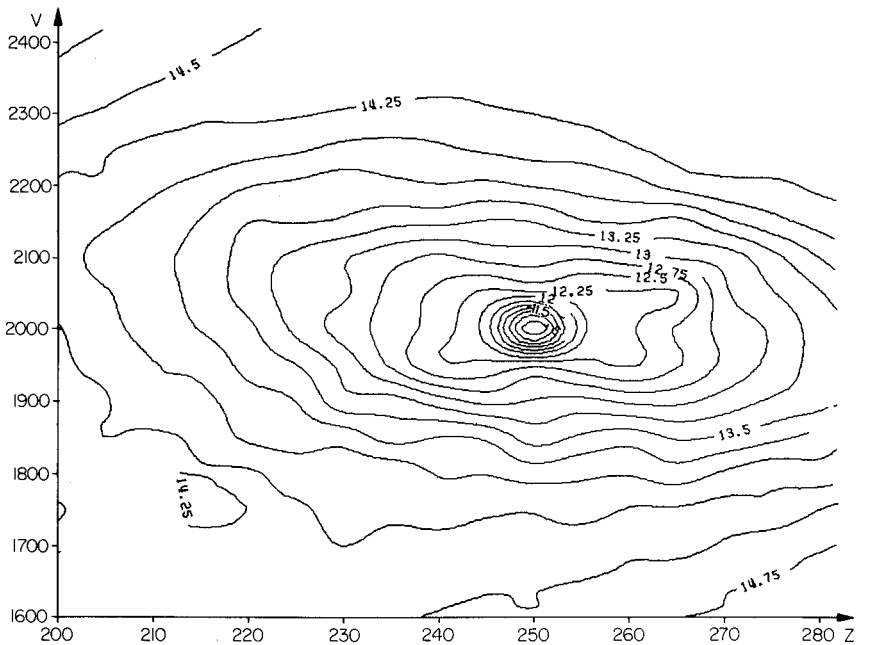

FIG. 4a. Contours of the objective function (3): large scale.

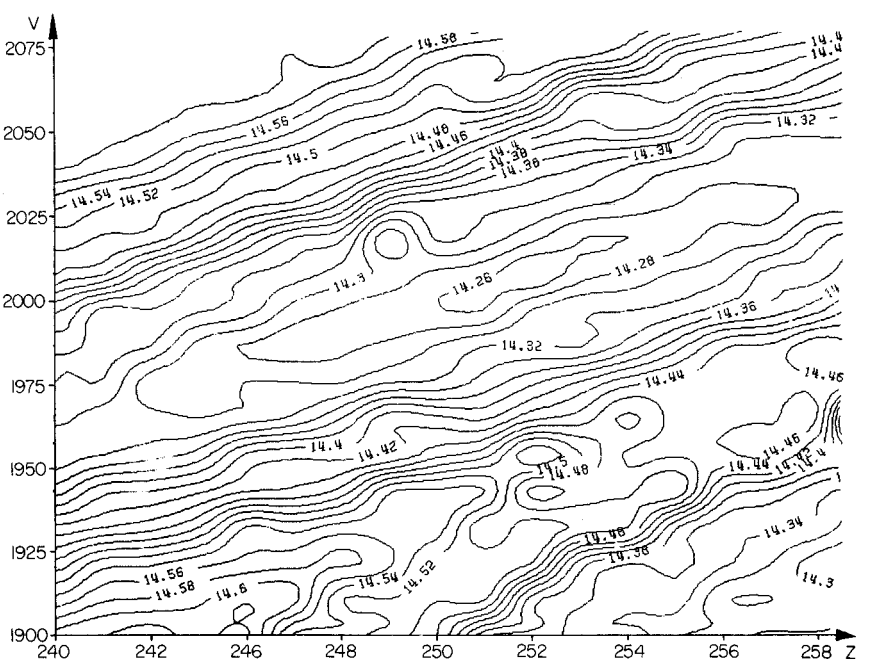

FIG. 4b. Contours of the objective function (3): large scale.

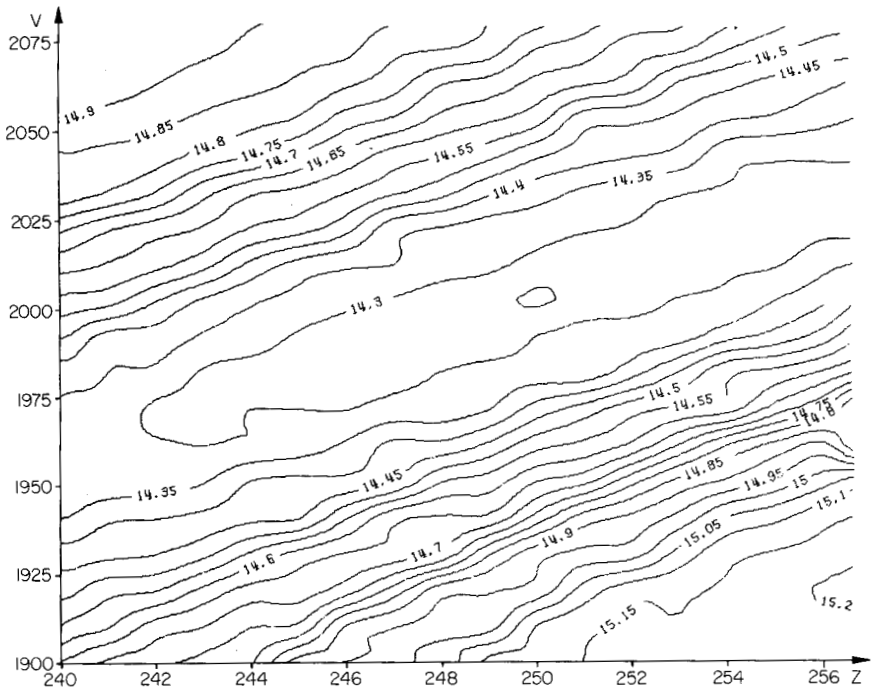

FIG. 5. Contours of the objective function (4).

traveltime curves. This undesirable phenomenon can be avoided by also considering the form of the wavelet. Let us change functional (3) in the following way:

$$S'_n(\theta) = \sum_{i=1}^{I} \frac{1}{K\,\Delta t} \sum_{k=1}^{K} \pm \frac{\{F(k\,\Delta t) \sum_{j=1}^{J} U_{ij}(\tau_{ijn}(\theta) + k\,\Delta t)\}^2}{J \sum_{j=1}^{J} U_{ij}^2(\tau_{ijn}(\theta) + k\,\Delta t)}, \tag{4}$$

where $F(t)$ is the known form of the signal.

The plus sign in this expression is chosen where a product in the numerator is positive (i.e. when the form of the signal and the average value of the wavefield calculated along the traveltime curve τ have the same sign at the sample k); where the reverse occurs, the minus sign is chosen. We can see that a product in the numerator expresses a simple weighting of the estimated signal when a form of the signal is taken as a weighting function. Numerical experiments show that the accuracy of parameter estimation using the objective function (4) depends only on the frequency of the signal $F(t)$ and not on its envelope.

The contours of the objective function $\psi' = -S'$ in the vicinity of the global minimum (on a small scale) are shown in Fig. 5. As we can see, local minima have disappeared.

We use a combination of the two objective functions (3) and (4). The semblance functional (3) is found to be a good tool for the estimation of the presence or absence of a correlated signal on the record section; therefore, it is used in the first

stage of the minimum search. The model parameters obtained from this stage are used as input for the second stage where the objective function (4) is used.

5. Minimization Algorithm

The method of minimization of the objective function is an important stage of the inversion algorithm. Many algorithms have been proposed to solve this problem (Himmelblau 1972; Gill and Murray 1974; Gill, Murray and Wright 1981). However, none of these algorithms has proved to be a universal solution for non-linear programming problems.

Numerical methods of optimization can be divided into two groups:

5.1. *Methods using derivatives*

One of these methods (the Gauss-Newton) has been used previously in geophysical applications (Bishop *et al.* 1985). In practice, the derivative-type methods have two main disadvantages. Firstly it is laborious, or sometimes impossible, to provide analytical functions for the derivatives. Although evaluation of the derivatives by different schemes can be substituted for evaluation of the analytical derivatives, the numerical error is introduced. Secondly, optimization techniques based on the evaluation of derivatives require relatively much preparation by the user before the problem can be introduced into the algorithm.

5.2. *Minimization methods without using derivatives*

More commonly known as the search methods of optimization, in these methods the directions for minimization are determined only from successive evaluations of the objective function. Methods using derivatives generally converge faster than direct search methods. However, because of the difficulties described, search optimization algorithms have been devised which may, in practice, prove to give better convergence than methods using derivatives.

To search for a parameter vector which minimizes the objective function we use an algorithm of flexible polyhedron search. This method was proposed by Nelder and Mead (Himmelblau 1972) to minimize a function of n independent variables using $(n + 1)$ vertices of a flexible polyhedron in E. (Regular polyhedrons in E are simplexes. For example: for two variables, the regular simplex is an equilateral triangle; for three variables, the regular simplex is a regular tetrahedron; etc.) This method can be briefly described as follows (Fig. 6): The vertex (point) which yields the highest value of the objective function is projected through the centre of gravity (centroid) of the remaining vertices. Improved (lower) values of the objective function are found by successively replacing the point with the highest value of objective function by a better point, until the minimum function is found. (For details of the algorithm, see Appendix.)

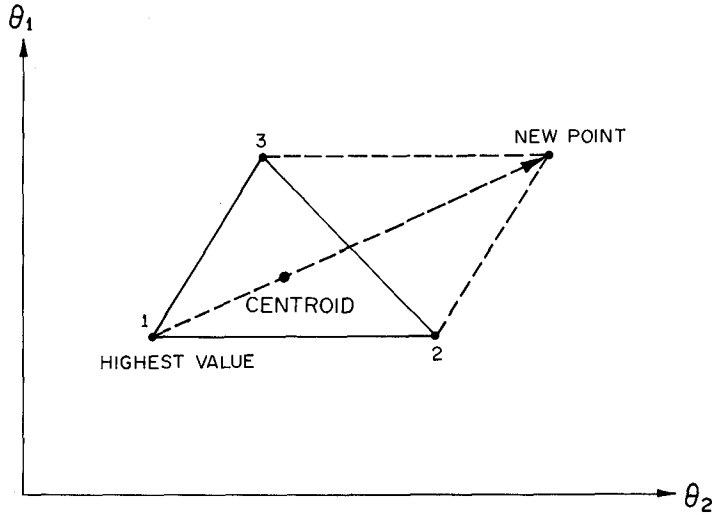

FIG. 6. Regular simplex for two variables. 1 denotes the largest value of the objective function; arrow pointing in the direction of function decrease.

5.3. *Local extrema*

In spite of our efforts to construct an objective function that contains only one minimum, the possibility remains that the optimization converges to a local minimum. Rothman (1985) developed a method of stack-power maximization by stochastic relaxation which has a high probability of finding the global maximum. An alternative approach is to run the program from random starting points.

6. EXAMPLES

We shall consider some examples illustrating the application of the inversion algorithm to synthetic and field data.

Example 1

Figure 7 shows the depth model with three layers. Velocities in the layers are $V_1 = 1500$ m/s, $V_2 = 1800$ m/s and $V_3 = 2100$ m/s. The geometry of the reflection interfaces is determined by cubic spline with nodes in the points X = 100 m, X = 400 m, X = 700 m, X = 1000 m (vertical lines on the figure). The computation of the synthetic CMP gathers for this model was performed using the well-known ray method.

Input data for the inversion consists of twenty CMP gathers within the range 100–1000 m with a significant amount of random noise. The estimated parameters include the interval velocities in all the layers and the depth in the spline knots. Inversion is performed layer after layer (five parameters for each layer).

The initial model was constructed using first-guess velocities (dotted values on the figure) and zero-offset times, t_0 obtained from CMP gathers. As we can see from

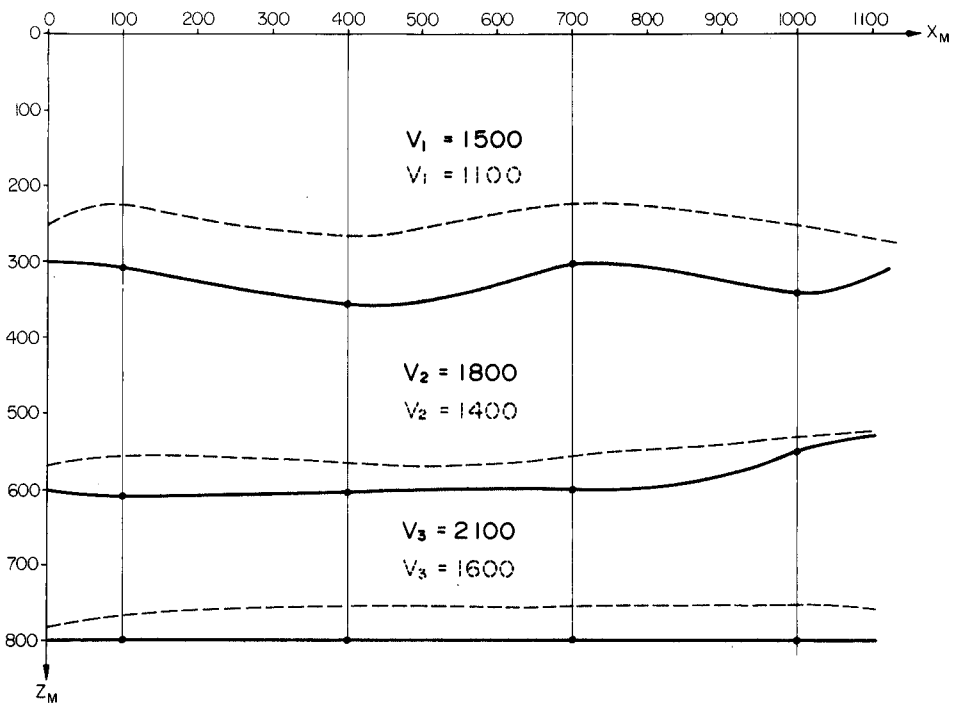

FIG. 7. Depth model (——), initial model (— — —). Result of inversion coincides with solid lines.

the figure, the difference between the true and initial models reaches 50 m in depth and 500 m/s in velocity (i.e. a deviation from the correct parameters of about 20%). The inversion algorithm converged to the solution after about 200 iterations for a layer.

Example 2

Let us now consider the application of the proposed inversion algorithm to a marine seismic line.

Figure 8 shows part of a time section of the line. Four dominant events can be seen: the first at about 1.65 s is the sea-bottom reflection, the second reflection at about 2.1 s is the Upper Yafo Formation, the third reflection at about 2.55 s is the Lower Yafo Formation and the fourth reflector at about 3.0 s is the top of the salt. All the events appear to be more or less horizontal and constancy of stacking velocities along the line indicates the constancy of the interval velocities. Input data for the inversion consist of 25 common shot gathers with shots every two stations beginning at station 840. Every gather consists of 48 traces with a group interval of 50 m and a minimum offset of 450 m.

Examples of some common shot seismograms are shown in Fig. 9; the signal-to-noise ratio is high and all four dominant events can be seen clearly. In this example,

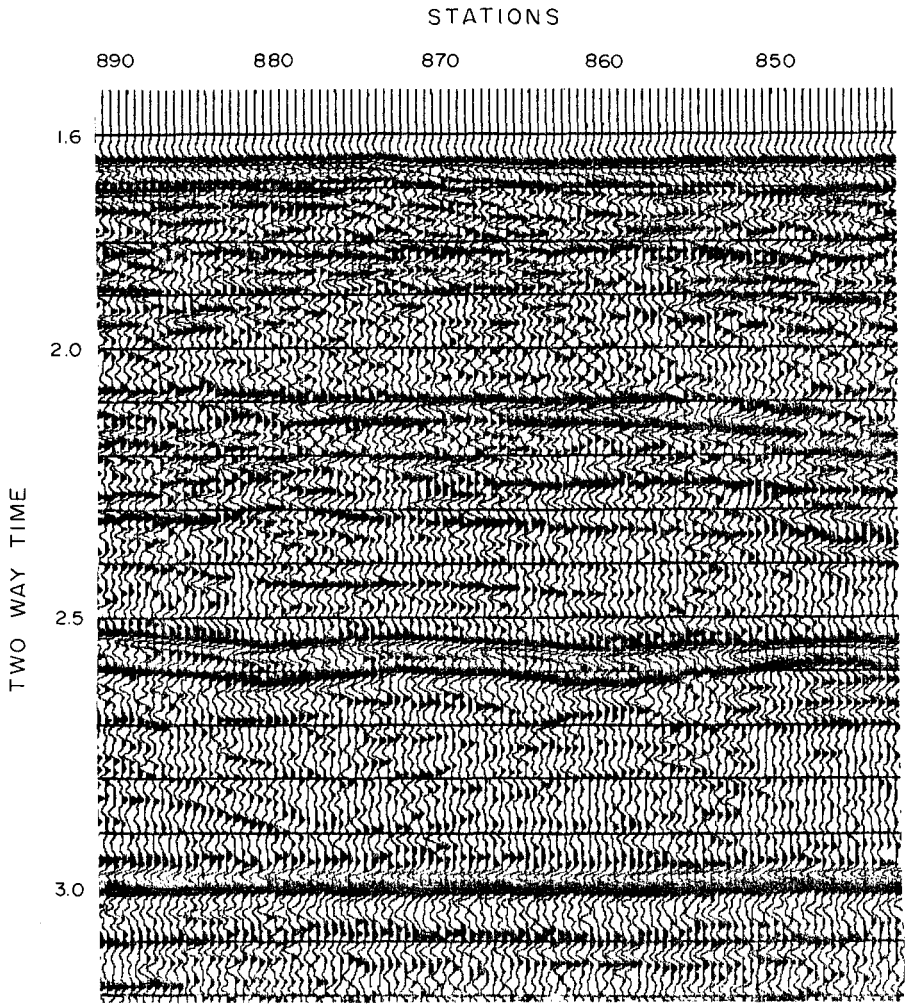

FIG. 8. Time section.

the first-guess model (broken lines on Fig. 10) was chosen to be significantly different from the model which can be obtained by applying the Dix formulae to t_0 and stacking velocities. This was done to check the convergence of the algorithm. The inversion algorithm attempts to maximize the coherency measure which was computed along the theoretical times by modifying the velocities and depths of the model.

Figure 10 shows the final velocity–depth model after about 200 iterations for each layer. Node points of the interfaces are depicted by black points in the figure. The differences between initial and final models reaches 25–30%. The results of inversion (interval velocities and thicknesses of the layer) are in good agreement with the results of conventional data interpretation (Mart and Ben Gai 1982).

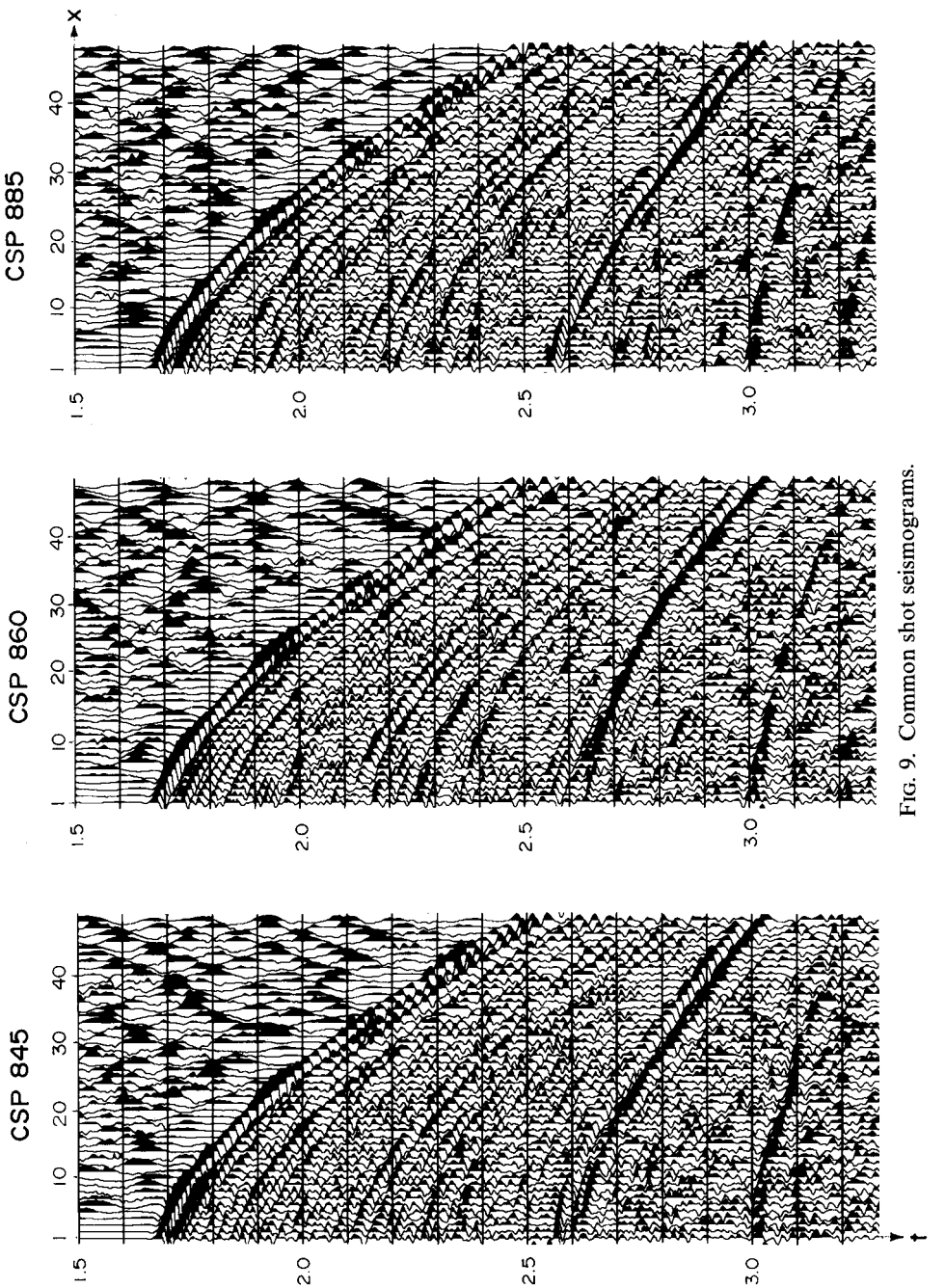

FIG. 9. Common shot seismograms.

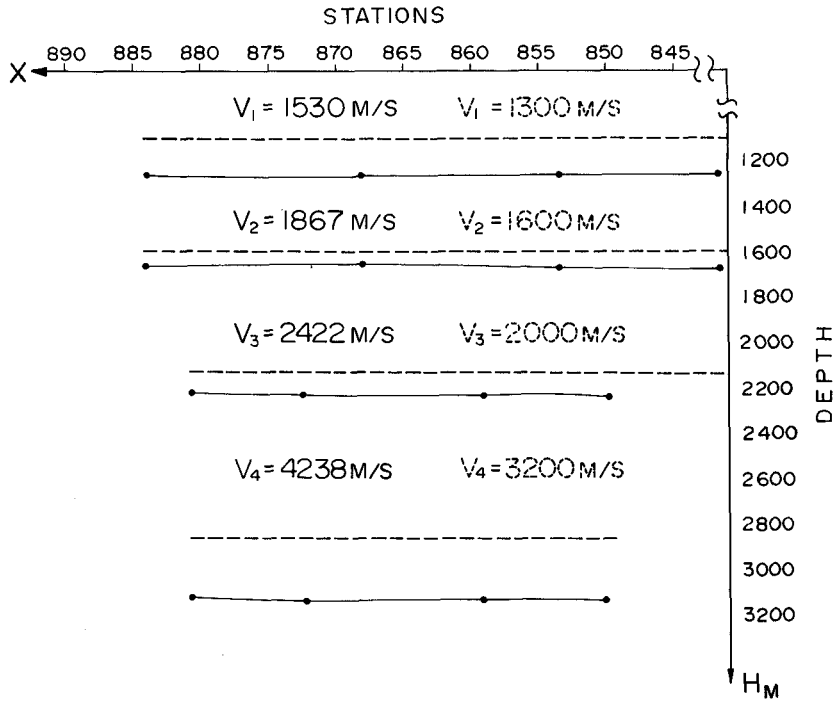

FIG. 10. Velocity–depth model (——) corresponds to time section on Fig. 8; (— — —) the first-guess model.

Example 3

Figure 11 shows part of a time section of the seismic line. Three events can be clearly seen at about 1.6–1.7 s, 2.4–2.6 s and 2.8–3.0 s. In this example the first event is a strong reflection with a small dip, the second and third reflections have a pronounced anticlinal character. Input data for inversion consists of thirty-two common shot gathers. The first shot station number is 156 and the last 218.

Figure 12 shows three common shot gathers. Each seismogram consists of twenty-four traces with a group interval of 70 m and a minimum offset of 245 m.

Figure 13 illustrates the result of inversion procedure. The inversion includes the determination of interval velocities in three layers and z-coordinates of four nodepoints for each layer. The nodepoints determine the cubic splines which represent the interfaces. Dotted lines in the figure show the initial model which was constructed using zero times for three major reflection events picked from the time section and stacking velocities. Solid lines in the figure show the final velocity–depth model which was obtained after about 200 iterations for each layer. Where the signal-to-noise ratio enables us to perform picking of the events, we can see that the traveltime curves derived from tracing rays through the final model practically coincide with those measured from common shot seismograms (Fig. 14).

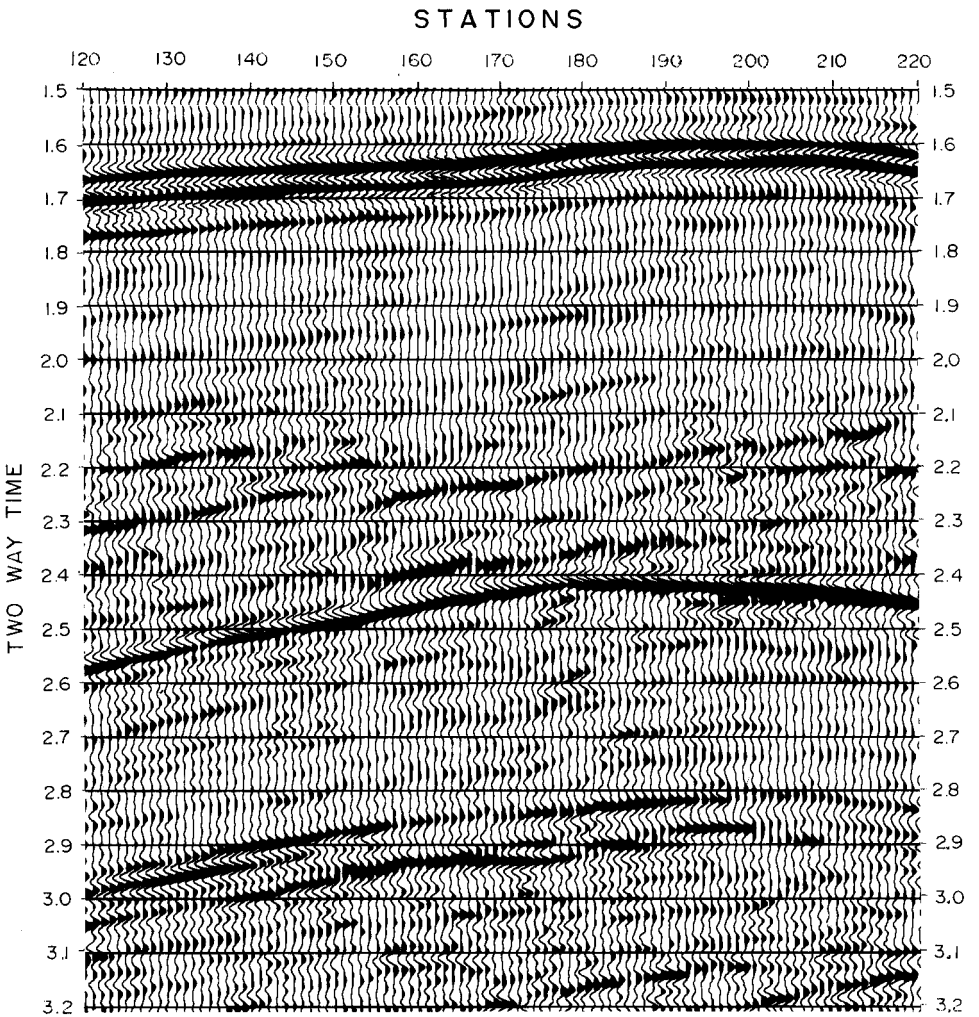

FIG. 11. Time section.

REMARKS

Several important questions remain to be answered: What value of coherency can be considered as a solution of the inversion algorithm? For a simple linear signal-noise model, the semblance coefficient is equal to a signal energy to total energy ratio (Neidell and Taner 1971). Therefore, the threshold value of coherency can be related to signal-to-noise ratio and, in practice, it is chosen empirically (as in velocity analysis). Small variations of the threshold cause small changes in the final results.

Another important question is that of computation efficiency. A good measure for this is the number of iterations. In our work 'an iteration' means one objective

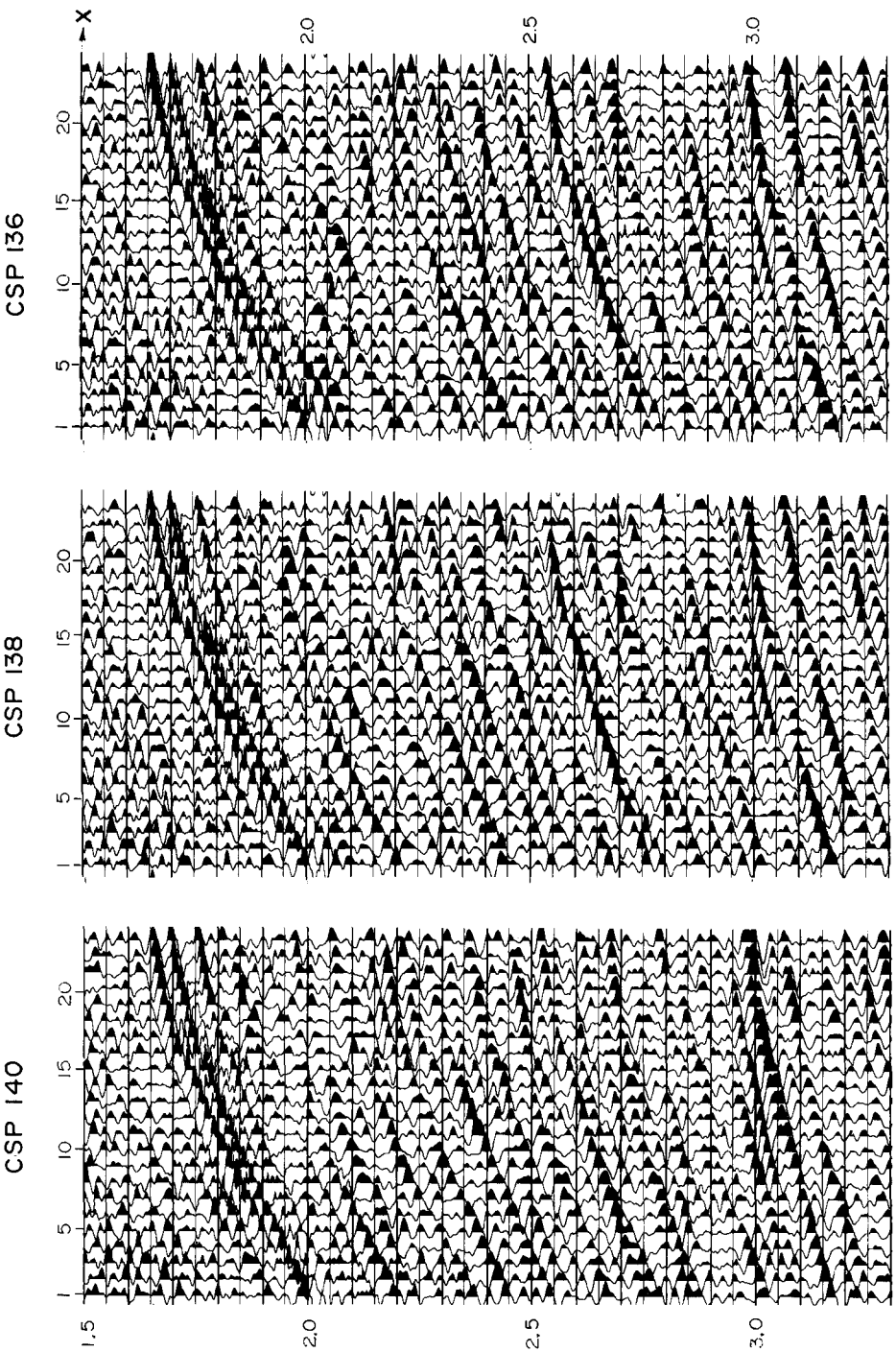

FIG. 12. Common shot seismograms.

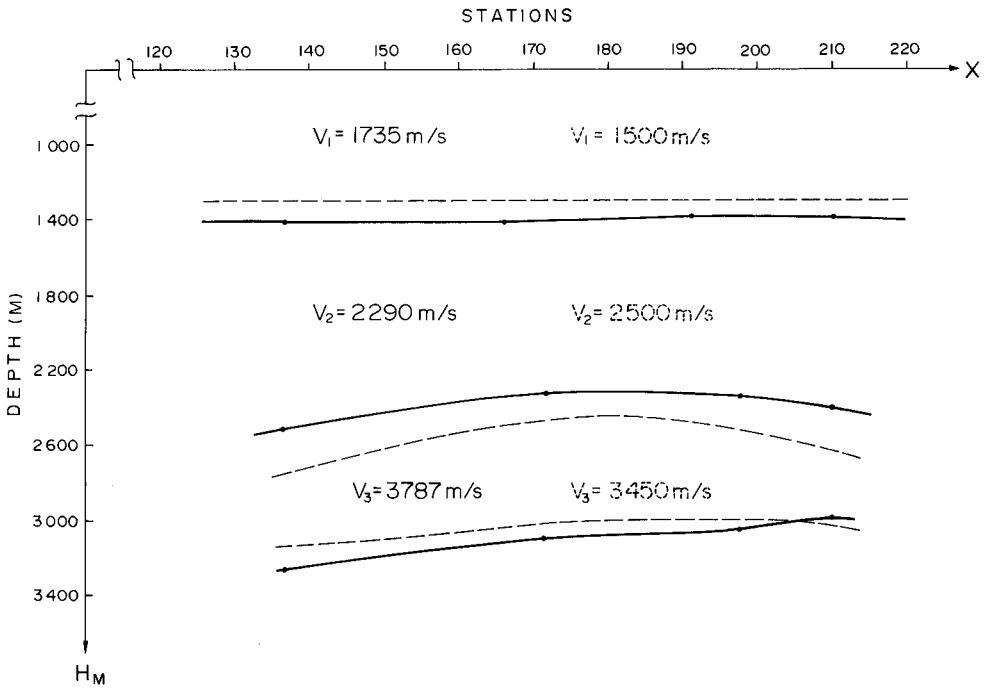

FIG. 13. Velocity–depth model (——) corresponds to time section on Fig. 10; (— — —) the first-guess model.

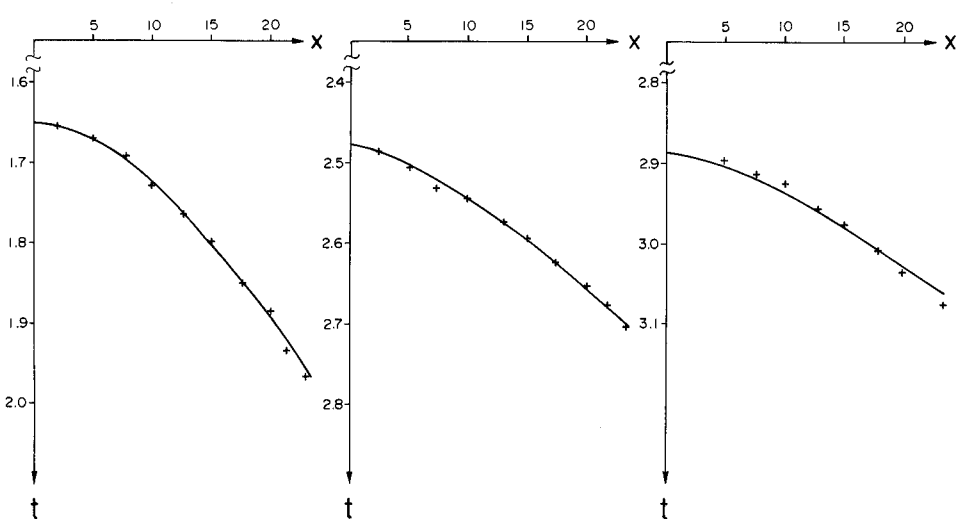

FIG. 14. Traveltime curves derived from tracing rays through the model (——) and measured from common shot seismogram (+ + +).

function evaluation (one ray-tracing cycle), whereas in some papers employing derivative methods, each iteration step consists of a numerical evaluation of the objective function derivatives with respect to the unknown parameters. In a non-linear case, the number of iterations can be significantly large (see e.g. Rothman (1985) where 4000 iterations are required for stack power maximization).

The number of iterations in non-linear methods depends on the minimization algorithm (the strategy of the search), the initial model and the termination criterion. Recent numerical experiments conducted after submission of this paper have successfully reduced the number of required iterations from about 200 to about 100 for each layer, a reduction which was achieved only by changing the termination criterion in the Nelder and Mead algorithm (see Appendix).

Conclusions

The proposed method of 'coherency' inversion is intermediate between full wave-field and tomographic inversions. It uses an optimization technique to estimate velocities and depths from unstacked seismic data. The method attempts to produce a velocity–depth model which maximizes some measure of coherency computed along traveltime curves derived from tracing rays through the model. The maximization is achieved using the Nelder and Mead method to modify an initial model and produce a number of model iterations. The initial model is constructed from well information or from results of conventional seismic processing. The proposed method has the advantage that picking times for selected reflectors on unstacked data is not required. The method has been successfully tested on synthetic data. The inversion was performed on two seismic lines and the estimated models agree well with known geological data.

Acknowledgements

We wish to thank the Earth Science Research Administration of the Ministry of Energy and Infrastructure for the grant which enabled us to carry out this work. We are grateful to the Institute for Petroleum Research and Geophysics for permission to publish this paper.

Appendix
Flexible Polyhedron Search (Himmelblau, 1972)

Let $\mathbf{X}_i^{(k)} = \{\chi_{i1}^{(k)}, \ldots, \chi_{ij}^{(k)}, \ldots, \chi_{in}^{(k)}\}^T$, $i = 1, \ldots, n+1$, be the ith vertex (point) in E^n on the kth stage of the search, $k = 0, 1, \ldots$ and let the value of the objective function at $\mathbf{X}_i^{(k)}$ be $f(\mathbf{X}_i^{(k)})$. We also need to label X vectors in the polyhedron that give the maximum and minimum values of $f(\mathbf{X})$. We define

$$f(\mathbf{X}_h^{(k)}) = \max \{f(\mathbf{X}_1^{(k)}), \ldots, f(\mathbf{X}_{n+1}^{(k)})\}$$

with the corresponding $\mathbf{X}_i^{(k)} = \mathbf{X}_h^{(k)}$, and

$$f(\mathbf{X}_S^{(k)}) = \min \{f(\mathbf{X}_1^{(k)}), \ldots, f(\mathbf{X}_{n+1}^{(k)})\}$$

with the corresponding $\mathbf{X}_i^{(k)} = \mathbf{X}_S^{(k)}$. Since the polyhedron in E^n comprises $(n+1)$ vertices, $\mathbf{X}_1, \ldots, \mathbf{X}_{n+1}$, let $\mathbf{X}_{n+2}$ be the centroid of all the vertices excluding X_h. The coordinates of the centroid are given by

$$\chi_{n+2,j}^{(k)} = \frac{1}{n}\left\{\left(\sum_{i=1}^{n+1} \chi_{ij}^{(k)}\right) - \chi_{hj}^{(k)}\right\} \quad j = 1, \ldots, n, \tag{A1}$$

where the index j designates each coordinate direction.

The initial polyhedron is usually selected to be a regular simplex (it does not have to be), with point S as the origin, or perhaps the centroid as the origin. The procedure of finding a vertex in E^n at which $f(X)$ has a better value involves four operations:

1. *Reflection*

Reflect $\mathbf{X}_h^{(k)}$ through the centroid by computing

$$\mathbf{X}_{n+3}^{(k)} = \mathbf{X}_{n+2}^{(k)} + \alpha(\mathbf{X}_{n+2}^{(k)} - \mathbf{X}_h^{(k)}, \tag{A2}$$

where $\alpha > 0$ is the reflection coefficient, $\mathbf{X}_{n+2}^{(k)}$ is the centroid computed by (A1), and $\mathbf{X}_h^{(k)}$ is the vertex at which $f(X)$ is the largest of $(n+1)$ values of $f(\mathbf{X})$ on the kth stage.

2. *Expansion*

If $f(\mathbf{X}_{n+3}^{(k)}) < f(\mathbf{X}_S^{(k)})$, expand the vector $(\mathbf{X}_{n+3}^{(k)} - \mathbf{X}_{n+2}^{(k)})$ by computing

$$X_{n+4}^{(k)} = \mathbf{X}_{n+2}^{(k)} + \gamma(X_{n+3}^{(k)} - \mathbf{X}_{n+2}^{(k)}), \tag{A3}$$

where $\gamma > 1$ is the expansion coefficient. If $f(\mathbf{X}_{n+4}^{(k)}) < f(\mathbf{X}_S^{(k)})$, replace $\mathbf{X}_h^{(k)}$ by $\mathbf{X}_{n+4}^{(k)}$ and continue from step 1 with $k = k+1$. Otherwise, replace $\mathbf{X}_h^{(k)}$ by $\mathbf{X}_{n+3}^{(k)}$ and continue from step 1 with $k = k+1$.

3. *Contractions*

If $f(\mathbf{X}_{n+3}^{(k)}) > f(\mathbf{X}_i^{(k)})$ for all $i \neq h$, contract the vector $(\mathbf{X}_h^{(k)} - \mathbf{X}_{n+2}^{(k)})$ by computing

$$\mathbf{X}_{n+5}^{(k)} = \mathbf{X}_{n+2}^{(k)} + \beta(\mathbf{X}_h^{(k)} - \mathbf{X}_{n+2}^{(k)}), \tag{A4}$$

where $0 < \beta < 1$ is the contraction coefficient. Replace $\mathbf{X}_h^{(k)}$ by $\mathbf{X}_{n+5}^{(k)}$ and return to step 1 to continue the search on the $(k+1)$ stage.

4. *Reduction*

If $f(\mathbf{X}_{n+3}^{(k)}) > f(\mathbf{X}_h^{(k)})$, reduce all the vectors $(\mathbf{X}_i^{(k)} - \mathbf{X}_S^{(k)})$, $i = 1, \ldots, n+1$, by one-half from $\mathbf{X}_S^{(k)}$ by computing

$$\mathbf{X}_i^{(k)} = \mathbf{X}_S^{(k)} + 0.5(\mathbf{X}_i^{(k)} - \mathbf{X}_S^{(k)}) \qquad i = 1, \ldots, n+1 \tag{A5}$$

and return to step 1 to continue the search on the $(k+1)$ stage.

The criterion used by Nelder and Mead (Himmelblau 1972) to terminate the search was to test whether

$$\left\{\frac{1}{n+1}\sum_{i=1}^{n+1}[f(\mathbf{X}_i^{(k)}) - f(\mathbf{X}_{n+2}^{(k)})]^2\right\}^{1/2} < \varepsilon, \tag{A6}$$

where ε is an arbitrarily small number, and $f(\mathbf{X}_{n+2}^{(k)})$ is the value of the objective function at the centroid $\mathbf{X}_{n+2}^{(k)}$.

The reflection coefficient α is used to project the vertex with the largest value of $f(\mathbf{X})$ through the centroid of the flexible polyhedron. The expansion coefficient γ is used to elongate the search vector if the reflection has produced a vertex with a value of $f(\mathbf{X})$ smaller than the smallest $f(\mathbf{X})$ obtained prior to the reflection. The contraction coefficient β is used to reduce the search vector if the reflection has not produced a vertex with a value of $f(\mathbf{X})$ smaller than the second largest value of $f(\mathbf{X})$ obtained prior to the reflection. Therefore, by means of either expansions or contractions, the size and shape of the flexible polyhedron are scaled to fit into the topography of the problem being solved. Nelder and Mead (Himmelblau 1972) recommended the values of $\alpha = 1$, $\beta = 0.5$ and $\gamma = 2$ as being generally satisfactory for minimization.

References

Berkhout, A.J. 1984. Multidimensional linearized inversion and seismic migration. *Geophysics* **49**, 1881–1895.

Bishop, T.N., Bube, K.P., Cutler, R.T., Langan, R.T., Love, P.L., Resnick, J.R., Shuey, R.T., Spindler, D.H. and Wyld, H.W. 1985. Tomographic determination of velocity and depth in laterally varying media. *Geophysics* **50**, 903–923.

Bleistein, N., Cohen, J.K. and Magin, F.G. 1985. Computational and asymptotic aspects of velocity inversion. *Geophysics* **50**, 1253–1265.

Clayton, R.W. and Stolt, R.H. 1981. A Born-WKBJ inversion method for acoustic reflection data. *Geophysics* **46**, 1559–1567.

Gauthier, O., Virieux, J. and Tarantola, A. 1986. Two-dimensional non-linear inversion of seismic wave-forms: numerical results. *Geophysics* **51**, 1387–1403.

Gill, P.E. and Murray, W. 1974. *Numerical Methods for Constrained Optimization.* Academic Press Inc.

Gill, P.E., Murray, W. and Wright, M.M. 1981. *Practical Optimization.* Academic Press Inc.

Gjoystdal, H. and Ursin, B. 1981. Inversion of reflection times in three dimensions. *Geophysics* **49**, 972–983.

Goldin, S.V. 1979. *Interpretation of Seismic Data.* Nedra, Moscow [in Russian]. English translation: *Seismic Translation Inversion*, 1986. SE8, Tulsa.

HIMMELBLAU, D.M. 1972. *Applied Nonlinear Programming*, 148–155. McGraw-Hill Book Co.

IKELLE, L.T., DIET, J.P. and TARANTOLA, A. 1986. Linearized inversion of multioffset seismic reflection data in the w–k domain. *Geophysics* **51**, 1266–1276.

KONG, S.M., PHINNEY, R.A. and ROY-CHOWDHURY, K. 1985. A nonlinear signal detector for enhancement of noisy seismic record sections. *Geophysics* **50**, 539–550.

MART, Y. and BEN GAI, Y. 1982. Some depositional patterns at continental margins of the southeastern Mediterranean Sea. *The American Association of Petroleum Geologists Bulletin* **66**, 460–470.

MCAULAY, A.D. 1985. Prestack inversion with plane-layer point-source modeling. *Geophysics* **50**, 77–89.

NEIDELL, N.S. and TANER, M.T. 1971. Semblance and other coherency measures for multichannel data. *Geophysics* **36**, 482–497.

RONEN, J. and CLAERBOUT, J.F. 1985. Surface-consistent residual statics estimation by stack-power maximization. *Geophysics* **50**, 2759–2767.

ROTHMAN, D. 1985. Nonlinear inversion, statistical mechanics and residual statics estimation. *Geophysics* **50**, 2784–2796.

STOLT, R.H. and WEGLEIN, A.B. 1985. Migration and inversion of seismic data. *Geophysics* **50**, 2458–2472.

TARANTOLA, A. 1984a. Linearized inversion of seismic reflection data. *Geophysical Prospecting* **32**, 998–1015.

TARANTOLA, A. 1984b. Inversion of seismic reflection data in the acoustic approximation. *Geophysics* **49**, 1259–1266.

TARANTOLA, A. 1986. A strategy for nonlinear elastic inversion of seismic reflection data. *Geophysics* **51**, 1893–1903.

TOLDI, J. 1985. Velocity analysis without picking. 55th SEG meeting, Washington D.C., Expanded Abstracts, 575–578.